Electronic Supplementary Material (ESI) for Nanoscale.

Supplemental Information for:

Effect of Substrate Discontinuities on the Propagating Surface Plasmon Polariton Modes in Gold Nanobars

Paul Johns,[*] Kuai Yu,[*] Mary Sajini Devadas, Zhongming Li, Todd A. Major, and Gregory V. Hartland[†]

Department of Chemistry and Biochemistry

University of Notre Dame

Notre Dame, IN 46556-5670

[*] These students contributed equally to this work.

[†] Corresponding author; e-mail: ghartlan@nd.edu

Additional scattered light, atomic force microscopy (AFM) and pump-probe microscopy images of gold nanobars suspended on trenches are presented in Figures S1 and S2. For the nanobar in Figure S1 there is a decrease in the SPP propagation length on the far side of the trench. In contrast, for the nanobar in Figure S2 the measured propagation length is similar on either side of the trench. For both nanobars, experiments were performed with pump laser excitation at either end.

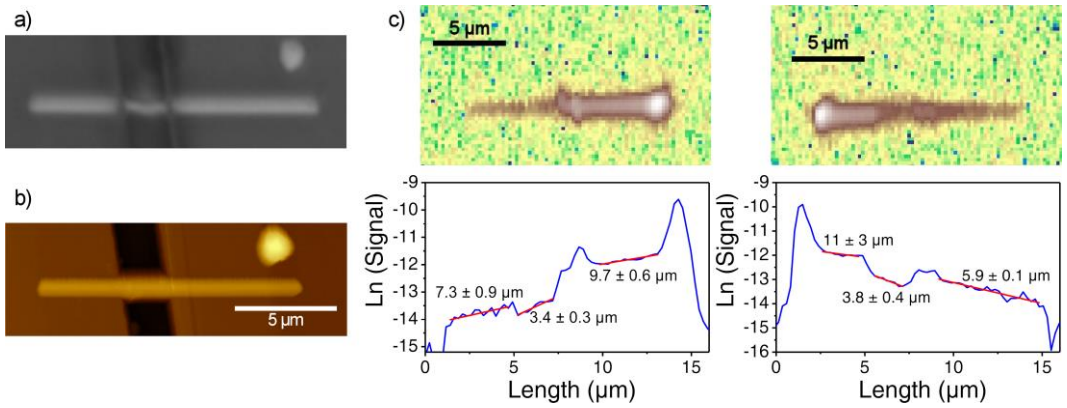

Figure S1: (a) Scattered light image of a suspended nanobar. (b) AFM image of the same nanobar. The nanobar has a length of 12.0 μm, and a height of 500 ± 10 nm. (c) Top panel: Transient absorption images recorded with the pump laser focused at either end of the nanobar. ~~(d)~~ Bottom panel: Line profiles extracted from the transient absorption images. The transient absorption data is presented on a log scale, and the red lines show fits to the data that yield the propagation length.

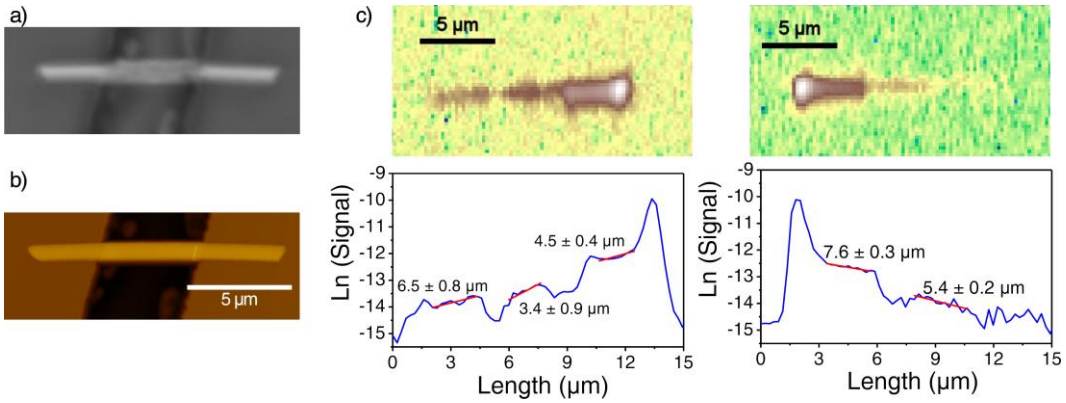

Figure S2: (a) Scattered light images of a suspended nanobar. (b) AFM image of the same nanobar. The nanobar has a length of 11.7 μm, and a height of 360 ± 10 nm. (c) Top panel: Transient absorption images recorded with the pump laser focused at either end of the nanobar. Bottom panel: ~~(d)~~ Line profiles extracted from the transient absorption images. The transient absorption data is presented on a log scale, and the red lines show fits to the data that yield the propagation length.

Figures S3 and S4 show the results of finite element simulations for nanobars with a square cross-section, and widths of 400 nm (Fig. S3) and 900 nm (Fig. S4). For the 900 nm wide nanobar, both the H_1 and H_3 modes appear for the supported nanobar, and the $E^{(1,1)}$ mode appears for the nanobar in air. The H_1 mode is localized at the nanobar-glass interface and, like what happens for the bound H_0 mode, as the gap between the nanobar and the glass increases, this mode transforms into a series of modes that involve the glass and the nanobar to varying degrees. For the 400 nm wide nanobar, we were not able to find the either the H_1, H_3 or $E^{(1,1)}$ modes, presumably because these modes suffer a cut-off at small sizes.

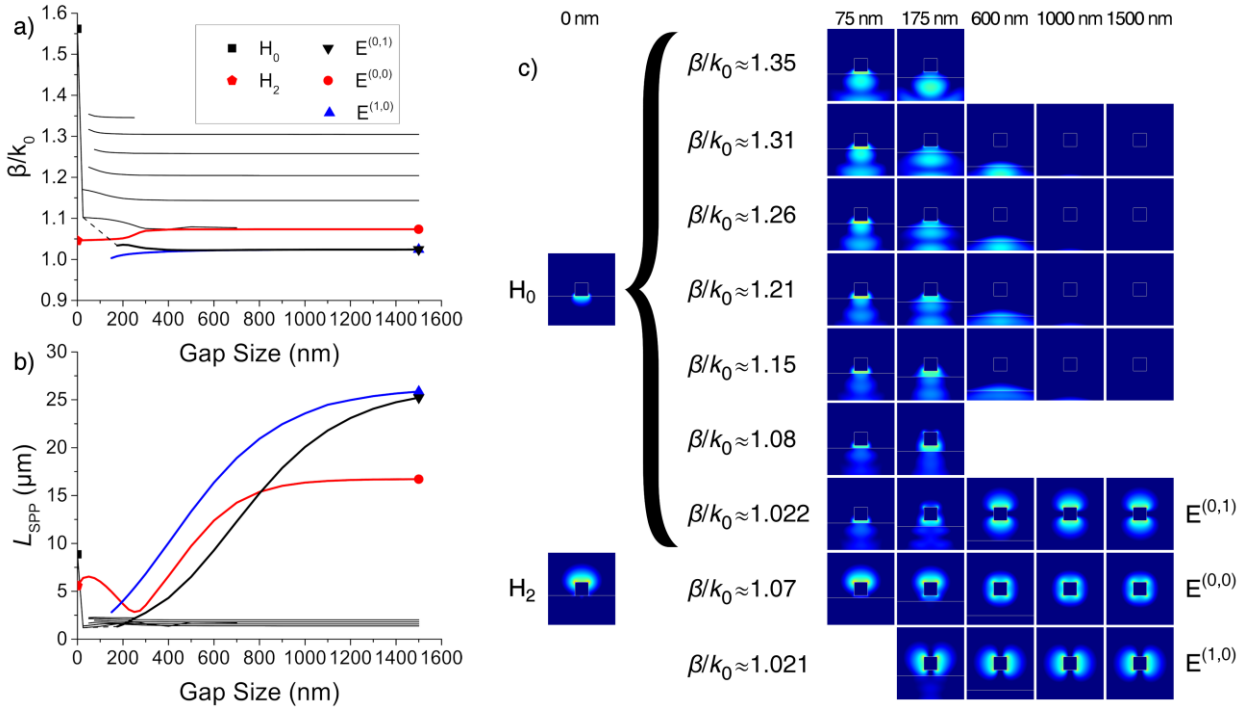

Figures S3: Plots of (a) the phase constant β/k_0, and (b) the propagation length L_{SPP} versus gap size for a gold nanobar with a square cross-section and a width of 400 nm. Panel (c) shows plots of the field distributions (on a log scale) for selected modes at different nanobar-surface gap sizes.

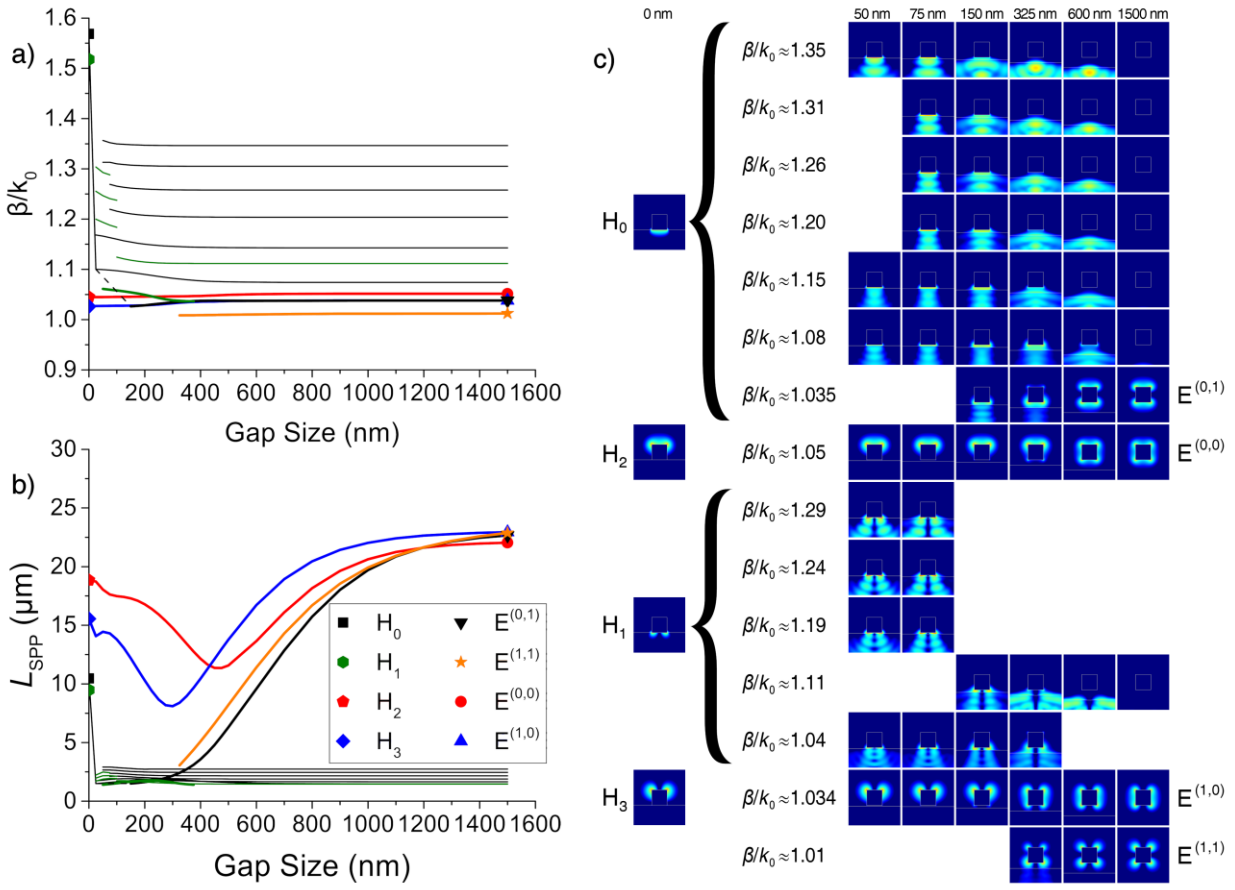

Figures S4: Plots of (a) the phase constant β/k_0, and (b) the propagation length L_{SPP} versus gap size for a gold nanobar with a square cross-section and a width of 900 nm. Panel (c) shows plots of the field distributions (on a log scale) for selected modes at different nanobar-surface gap sizes.

The behavior of the bound (H_0) and leaky (H_2) modes for the nanobars in Figures S3 and S4 are very similar to that for the 600 nm nanobars discussed in the main text. The leaky mode transforms into the $E^{(0,0)}$ mode as the gap size increases, and the bound mode transforms into a series of modes that involve the glass and the nanobar. For this series of modes, the mode with the major contribution from the nanobar eventually becomes the $E^{(0,1)}$ mode at large gap sizes. Importantly, all the modes that are connected to the bound mode are strongly damped for the gap sizes relevant to our experiments (which is a few hundred nanometers). Thus, the exact dimensions of the nanobar do not affect the analysis presented in the main text of the manuscript.

Scanning Electron Microscope (SEM) images of select nanobars are presented in Figure S5. Additional SEM images are presented in the Supporting Information of Ref. [27] of the main text (K. Yu, M. S. Devadas, T. A. Major, S. S. Lo and G. V. Hartland, *J. Phys. Chem. C*, 2014, 118, 8603-8609). The images show that a variety of different shapes are present, although a majority of the nanobars have roughly rectangular cross-sections.

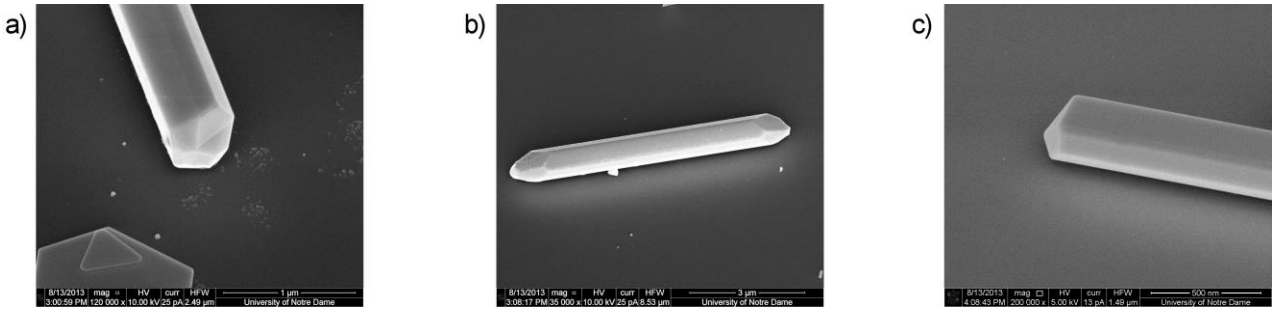

Figure S5. SEM images (a-c) of select chemically synthesized gold nanobars. These nanobars are facetted, with unsymmetrical cross-sections that have apexes that lie above the surface.